A pair potentials study of matrix-isolated atomic zinc. I. Excited $^1P_1$ state dynamics in solid Ar

P. N. Kerins
Department of Chemistry, National University of Ireland, Maynooth, Co. Kildare, Ireland

John G. McCaffrey[a)]
Department of Chemistry, University of Utah, Salt Lake City, Utah 84112

(Received 6 April 1998; accepted 19 May 1998)

The pair-potentials calculations of McCaffrey and Kerins [J. Chem. Phys. **106**, 7885 (1997)] used with success in simulating the emission spectroscopy of the Zn–RG matrix systems are extended to examine the different temporal decay characteristics exhibited at low temperature, $T<13$ K, by the singlet emission bands in the Zn–Ar matrix system. The 238 nm band, assigned in the earlier theoretical work to the body mode Q_2, exhibits a 0.1 ns risetime, the 219 nm band assigned to the waist mode Q_3, is prompt. By extracting the gradients and the second derivatives of the Q_3 and Q_2 mode potentials of a $Zn\cdot Ar_{18}$ cluster, decay rates of 3 and 2 ps, respectively, are calculated at the Franck–Condon regions of these potentials accessed in absorption, leading to effective competition between the Q_2 and Q_3 modes for relaxation of excited-state population and thereby to the coexistence of the 238 nm emission with the 219 nm band. A quasi-bound region is located at 0.32 Å in the body mode, Q_2, which slows down the relaxation on this mode and is identified as responsible for the recorded risetime on the 238 nm emission. The temperature dependence exhibited in the Zn–Ar system at higher temperatures ($T>14$ K) in which the intensity of the 219 nm band can reversibly be put into the 238 nm band, was examined by generating the (PES) potential-energy surface for coupled $Q_2\times Q_3$ vibronic modes. The theoretically predicted activation energy barrier is 380 cm^{-1}, which is only in qualitative agreement with the value of 130.6 cm^{-1} extracted in the kinetics study. Possible reasons for the overestimation in the theoretical value are discussed. © *1998 American Institute of Physics.* [S0021-9606(98)00432-2]

I. INTRODUCTION

Early attempts[1] at understanding the spectroscopy of atoms isolated in low-temperature solids were hampered because of the lack of reliable guest–host interaction potentials. In more recent times,[2] however, the availability of accurate experimental[3] and theoretical[4] potentials for metal atom–rare-gas atom diatomics as well as methods[5] for handling the complex interactions[6] occurring on the excited-state surfaces of atoms isolated in rare-gas clusters,[7] have allowed the successful simulation[8] of the optical spectroscopy of matrix-isolated metal atoms. In particular, the luminescence of atomic zinc isolated in the solid rare gases has been examined in detail both experimentally and from a pair potentials approach.

Using accurate, experimentally determined Zn·RG and RG·RG pair potentials, McCaffrey and Kerins[8] exploited the intrinsic fourfold symmetry of the cubooctahedral substitutional site, in which the zinc atom resides in the solid rare gases, to develop a simple $Zn\cdot RG_{18}$ cluster model which simulated successfully the pairs of emission bands observed in the Zn–RG matrix systems. The two vibronic motions[9] illustrated in the lower panel of Fig. 1 were identified as being responsible for the production of the pairs of emission bands following photoexcitation of the $4p\ ^1P_1-4s\ ^1S_0$ absorption band. The first motion, an in-phase contraction of 4 rare-gas atoms on a plane towards the zinc atom, referred to as the ''waist'' mode Q_3, produced the higher energy B emission band. The other, motion of the guest zinc atom towards one of the two octahedral interstitial sites adjacent to the substitutional site occupied in the ground state, the ''body'' mode Q_2, resulting in the lower energy C band. From the close agreement found between the spectral positions of the observed[10] and predicted[8] emission band maxima, it was concluded[8] that the simple $Zn\cdot RG_{18}$ cluster model developed, accounted for the pairs of emission bands present in the Zn–Ar, Zn–Kr, and Zn–Xe systems. Moreover, it was concluded that the interaction between the atomic zinc guest and the rare-gas host is dominated by localized, short-range forces and that these two lattice modes determine the luminescence in the Zn–RG matrix systems.

In the present contribution the pair-potentials calculations of Ref. 8 are extended to check their efficacy in predicting the temperature dependence observed in a previously published kinetic study[11] of the luminescence in the Zn–Ar system. A summary of the luminescence spectroscopy in the Zn–Ar system is presented in Fig. 2 for an annealed sample at 9 K. Excitation into the $4p\ ^1P_1-4s\ ^1S_0$ absorption band, indicated by A in Fig. 2, produces the pair of emission bands at 219 and 238 nm labeled B and C. From lifetime measurements[10] *both* emission bands have been assigned to

[a)]Visiting Associate Professor 1998. Permanent address: Department of Chemistry, National University of Ireland, Maynooth, Co. Kildare, Ireland.

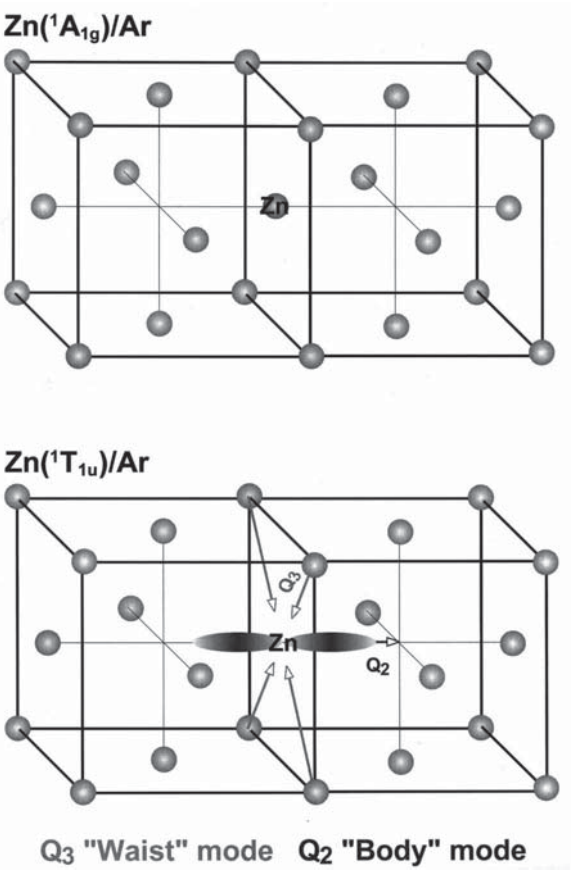

FIG. 1. Diagrams showing the behavior of atomic zinc isolated in a substitutional site of a solid Ar lattice in the ground singlet $^1A_{1g}$ electronic state and in the excited $^1T_{1u}$ electronic state. Two unit cells are shown to illustrate the relationship between the 12 nearest-neighbor Ar atoms surrounding the guest zinc atom located in a substitutional site and the framework of the fcc Ar lattice. Only 2 of the 6 atoms in the second surrounding sphere are shown in the Figure. The two shown are located in the center of the two end faces, the missing four would be positioned on the central vertical plane containing the Zn atom at a distance of the lattice parameter *a*. Illustrated in the lower panel are the atomic motions involved in the two lattice modes (Q_2 and Q_3) active in the excited state which dominate the luminescence spectroscopy.

the $4p\ ^1P_1 \rightarrow 4s\ ^1S_0$ transition of atomic zinc. The pair-potentials simulation of Ref. 8 indicated that the 219 nm emission band was associated with the waist mode Q_3, the 239 nm band with the body mode Q_2.

The previously mentioned kinetics study[11] provided a wealth of information on the dynamics occurring on the excited $^1P_1$ state surface of atomic zinc isolated in solid Ar. Thus on closer scrutiny of the temporal decay characteristics of the 238 nm emission it was noticed[11] that a risetime component, on the order of 0.1 ns, was present at low temperatures, $T<13$ K. Evidence for the existence of this risetime in the temporal decay profile of the *C* emission band is presented in Fig. 3. In the panel on the bottom right of Fig. 3, the recorded decay profile of the 238 nm band is shown compared with a fit which includes a decay and risetime (solid trace) and a simulation done only with the decaytime (grey trace). The contribution the risetime makes in the overall temporal profile of the 238 nm emission is the difference between the grey trace and the recorded data shown by dots. It results in the curvature present in the 238 nm decay curve,

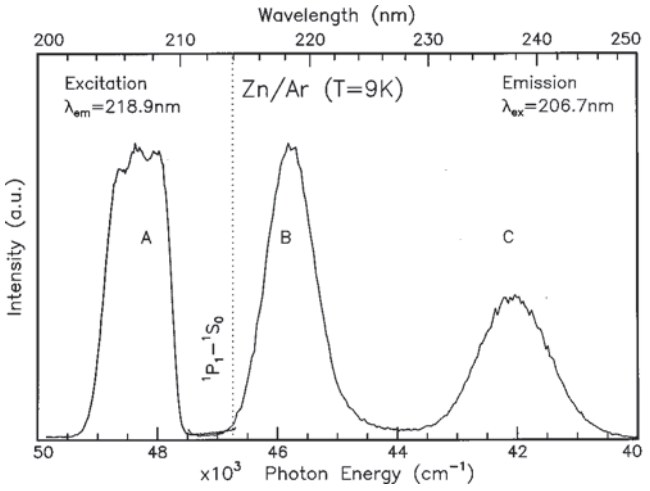

FIG. 2. A summary of the luminescence (excitation/emission) spectroscopy recorded at 9 K (Ref. 10) in an annealed 1/5000 Zn–Ar sample. The line position of the gas-phase singlet $4p\ ^1P_1-4s\ ^1S_0$ transition of atomic zinc is shown for comparison with the bands observed in the matrix.

shown on the bottom left in Fig. 3, which is clearly absent in the 219 nm decay curve, shown on the left, recorded at the same temperature and excitation wavelength.

From an analysis of the kinetics[11] it can be concluded, because of the presence of a risetime on the *C* emission band

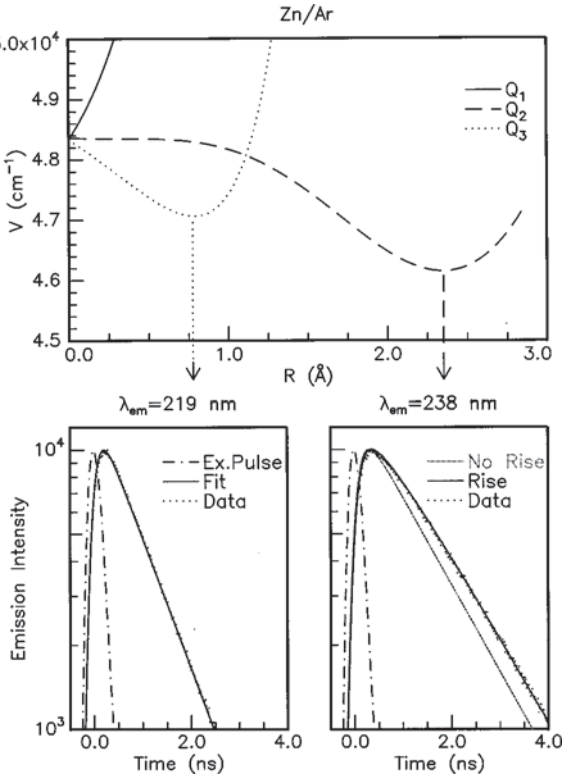

FIG. 3. Comparison of the potential energies calculated for displacements, *R*, along the breathing, body, and waist modes (Q_1, Q_2, and Q_3, respectively) in the excited $^1P_1$ electronic state of the Zn–Ar system. The panels on the bottom left and right show the recorded temporal decay profiles of the 219 and 238 nm emission bands arising from the waist and body modes, respectively. The time structure of the synchrotron radiation, used as the excitation pulse, is shown by the dot–dash lines in both panels. The presence of a risetime is evident in the body mode emission, shown on the lower right, and absent in the waist mode, lower left.

TABLE I. Morse $D_e[1-e^{-\beta(R-R_e)}]^2$ and repulsive exponential $Ae^{-\beta(R)}$ functions used as bound and free state pair potentials, respectively, for rare-gas–rare-gas interactions and atomic zinc–rare-gas atom interactions. Data is that quoted in Ref. 4.

Diatomic	D_e (cm^{-1})	R_e (Å)	β($Å^{-1}$)	$A(\times 10^{-6}$ $cm^{-1})$
Ar–Ar($X\ ^1\Sigma$)	99.2	3.761	1.685	⋯
ZnAr($X\ ^1\Sigma$)	95	4.18	1.001[a]	⋯
ZnAr($^1\Pi$)	700	2.97	1.429	⋯
ZnAr($^1\Sigma$)	⋯	⋯	1.615	0.50

[a]The β coefficient of ground state Zn·Ar is obtained by extrapolating the corresponding Zn·Kr and Zn·Xe values based on the trends exhibited in the $X\ ^1\Sigma$ states of the RG–RG systems for which more accurate data is available.

and its absence on the *B* emission band, that an intermediate level, or a rate determining step, must exist in the channel feeding the *C* emission band since both emission bands are produced from the same excitation. Specifically, the origin of the risetime component at low temperatures ($T<14$ K) in the *C* emission at 238 nm (the body mode) and its absence in the *B* emission at 219 nm (the waist mode) will be examined in the present work by calculating the gradients and the second derivatives of the body and waist mode potentials.

At higher temperatures ($T>14$ K) it was observed that an activated process converts the *B* into the *C* emission band on the spin singlet surface of the Zn–Ar system. From an Arrhenius plot of the nonradiative rates extracted in the Zn–Ar kinetics study[11] it was shown that this process involved a barrier of 130.6 cm^{-1}. The origin of the temperature dependent interconversion of the two bands at higher temperatures will also be examined from the calculated excited-state potentials. In the Zn–Ar system, spin singlet to triplet intersystem crossing (ISC) does not occur,[10] so it is anticipated that the temperature-dependent processes occurring on the pure spin singlet surface can, in this system, be studied in isolation from the complications introduced by crossings with the lower spin triplet surface. All of the other Zn–RG systems exhibit ISC and a pair potentials study of crossings with the lower spin triplet states is the topic of the article[12] following.

II. METHODS

A. Theoretical simulations

Details of the theoretical method used have already been published[8] so presentation here will be restricted to a summary. The $X\ ^1\Sigma_0$ ground state interaction potentials of the Zn·Ar and Ar_2 diatomics are described by Morse functions whose parameters have been extracted from spectroscopic measurements and are collected in Table I. Similarly, molecular constants of the bound excited $^1\Pi_1\mathrm{Zn}(p_x,p_y)\cdot\mathrm{Ar}$ state potential, $V_{1_\Pi}(R)$, have been obtained from experimental data and are described by a Morse function. The repulsive excited $^1\Sigma_0\mathrm{Zn}(p_z)\cdot\mathrm{Ar}$ state potential, $V_{1_\Sigma}(R)$, is described by a repulsive exponential function which was obtained from *ab initio* calculations.[3] In all the matrix calculations performed the ground-state zinc atom occupies, as depicted in the upper portion of Fig. 1, a substitutional site in the face centered cubic, fcc, packing structure of the argon lattice. The matrix calculations were performed for a quasi-molecular $\mathrm{Zn}\cdot\mathrm{Ar}_{18}$ cluster species composed of the 12 nearest-neighbor argon atoms in the first sphere surrounding the zinc atom in the substitutional site as well as the six atoms in the second surrounding sphere.

The general expressions[5,8] for the energies of the bound $^1A_1(p_z)$ state and the repulsive $^1E(p_x,p_y)$ states of the Zn–Ar matrix system are the following sums of Zn·Ar pair potentials:

$$W_{1_{A1}}(R)=\sum_{j=1}^{n}\left[\cos^2\theta_j V_{1_\Sigma}(R_j)+\sin^2\theta_j V_{1_\Pi}(R_j)\right], \quad (1)$$

$$W_{1_E}(R)=\sum_{j=1}^{n}\left[\sin^2\theta_j V_{1_\Sigma}(R_j)+(\cos^2\theta_j+1)V_{1_\Pi}(R_j)\right], \quad (2)$$

in which $V_{1_\Pi}(R)$ and $V_{1_\Sigma}(R)$ are the bound and repulsive excited singlet *p*-state potentials respectively of the diatomic Zn-Ar molecule.

As mentioned in the Introduction, the matrix calculations exploit the cubooctahedral symmetry of substitutional sites in the fcc lattice of the solid rare gases. Having fourfold symmetry it can be shown[8] that the summations in the general expressions given in Eqs. (1) and (2) can be replaced by the following products:

$$W_{1_{A1}}(R)=4[\cos^2\theta V_{1_\Sigma}(R)+\sin^2\theta V_{1_\Pi}(R)], \quad (3)$$

$$W_{1_E}(R)=2[\sin^2\theta V_{1_\Sigma}(R)+(\cos^2\theta+1)V_{1_\Pi}(R)], \quad (4)$$

for substitutional site occupancy of atomic zinc. In Eqs. (3) and (4), θ is the angle between the axis of atomic zinc motion, the central line on which the Zn atom is located in Fig. 1 referred to as the ''crystal axis,'' and the position of the rare-gas atoms in the fcc lattice. The 18 argon atoms in the $\mathrm{Zn}\cdot\mathrm{Ar}_{18}$ cluster used to represent the lattice are identified as belonging to four categories. The first group, has four atoms located on a plane perpendicular to the ''crystal axis,'' at a nearest-neighbor distance ($R=a/\sqrt{2}$, where a is the lattice parameter of the unit cell, 5.31 Å) from the guest zinc atom. The second group, consisting of five atoms, surround an octahedral interstitial site located on the crystal axis at a distance of half a lattice parameter ($R=a/2$) from the substitutional site accommodating the zinc atom in the ground state. An equivalent set of five atoms is located on the opposite side of the crystal axis. The last category consists of four four rare-gas atoms located on the same plane as category one atoms but at a distance of the lattice parameter ($R=a$) from the zinc atom.

The waist mode, Q_3, calculations are rather direct as the only variable involved is the distance of category one atoms from the zinc atom. The other atoms contribute a constant amount to the total energy but they do not vary in position during this mode. For the body mode, Q_2, the distances and angles to each of the four groups of rare-gas atoms are variables and it is the sum of all these contributions[8] which gives the total energy of the body mode.

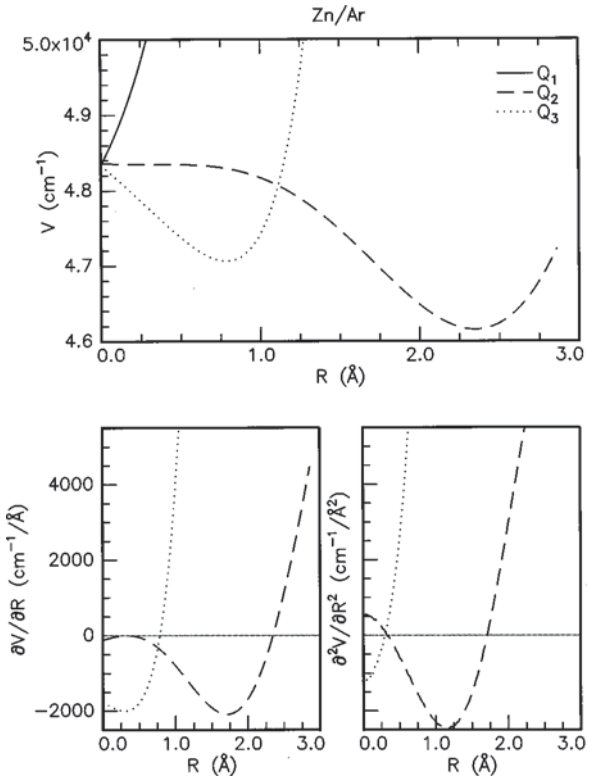

FIG. 4. Comparison of the breathing, body, and waist modes potentials (Q_1, Q_2, and Q_3, respectively) for the excited $^1P_1$ electronic state of the Zn–Ar system. The panels on the bottom left and right show the gradients and second derivatives of the body and waist mode potentials. For the three modes shown, R represents displacement from the substitutional site occupancy, $R=0$. The curve legend shown in the upper right is used consistently throughout the Figure.

III. RESULTS AND DISCUSSION

A. Low temperature

A clue to the origin of the risetime on the decay profile of the lower energy 238 nm emission band (body mode, Q_2) and its absence on the higher energy 219 nm emission band (waist mode, Q_3) can be found by comparing the shapes of the body and waist mode potentials, $V(R)$, in the Franck–Condon accessible regions from the substitutional site occupied by the zinc atom in the $^1S_0$ ground electronic state. On the plot shown in the top Panel of Fig. 3 this region is centered at $R=0.0$ Å. It is evident in Fig. 3 that the slope on the waist mode, Q_3 (dotted line), is considerably steeper here than that on the body mode, Q_2 (dashed line), which appears flat for small (<0.7 Å) displacement. It should be noted that the breathing mode, Q_1 which is also shown in the top panel of Fig. 3, will only play a role in absorption and not in thermally relaxed emission as both the body and waist modes lead to a lowering of energy while the breathing mode does not. To examine the differences in the body and waist modes in more detail, we extract the momenta and forces of the calculated Q_2 and Q_3 potentials from their gradients and second derivatives, respectively. On the bottom left of Fig. 4 the calculated gradients, $\partial V(R)/\partial R$, of the body and waist mode potentials of the Zn($^1P_1$)/Ar matrix system are compared. The second derivatives, $\partial^2 V(R)/\partial R^2$, of the two modes are compared on the bottom right in Fig. 4.

The gradient on the waist mode, Q_3, is negative with respect to displacement from the substitutional site occupied in the ground state, indicating that the excited-state geometry initially accessed in absorption is unstable. Using the minimum value of the second derivative for this mode, (-1289.1 cm^{-1}/Å^2 at $R=0$) and the reduced mass[13] of the 4 Ar atoms contracting in-phase towards the Zn atom, an *imaginary* frequency of 33 cm^{-1} is obtained assuming harmonic oscillator behavior for this mode. This corresponds to a time constant of ~1 ps which is consistent with the lack of a risetime detected for the 219 nm emission band on the 120 ps temporal resolution of the synchrotron radiation used in the experimental[11] work.

Similar to the waist mode, the body mode, Q_2, potential initially exhibits a negative, albeit much smaller, gradient at $R=0$ indicating that the Franck–Condon region accessed in absorption is also unstable. The second derivative calculated at $R=0$ is 575 cm^{-1}/Å^2 which yields a vibrational frequency of 17.3 cm^{-1} and an associated time constant of 1.93 ps. The competitive decay rates of 2 and 1 ps calculated at $R=0$ for the body Q_2 and waist Q_3 vibronic modes, respectively, leads to effective competition between these two modes for relaxation of excited-state population, and thereby, to the coexistence of the *C* band (238 nm) emission with the *B* band (219 nm).

However, as indicated by the dashed line in Fig. 4, the behavior of the body mode potential is much more complex for larger values of *R* than that of the waist mode. Details of the initial region of the body mode, Q_2, potential are shown in Fig. 5 on an expanded energy and distance scale as well as the gradient and second derivative. From the panel shown on

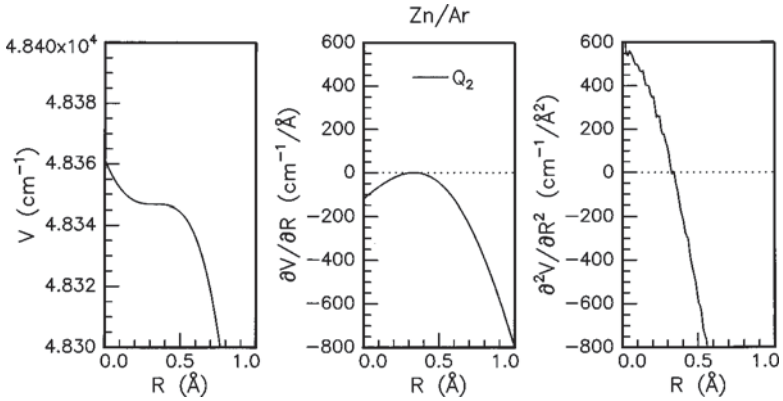

FIG. 5. Details of the body mode potential Q_2 in the Zn($^1P_1$)/Ar system. From left to right the energy, gradient, and second derivative of this mode are depicted.

the left in Fig. 5, it can be seen that the body mode potential, Q_2, drops rapidly from $R=0.0$ to $R=0.2$ Å, but from this latter point to 0.5 Å, it flattens off. As shown in the middle panel of Fig. 5, the gradient of the body mode at $R=0.32$ Å drops to zero, before going to very large negative values with increasing R. The second derivative calculated at $R=0.32$ Å is $19.53\ \mathrm{cm}^{-1}/\mathrm{Å}^2$. Once again assuming harmonic oscillator behavior at this local minimum and considering that the motion involved in the body mode is that of atomic zinc, a *real* frequency of $3.2\ \mathrm{cm}^{-1}$ is obtained. This corresponds to a vibrational period of 10.5 ps on what appears to be a quasi-bound portion of the body mode potential.

Comparing the time constants of the body and waist modes is rather difficult as the Q_2 mode has a quasi-bound portion while the Q_3 mode is free. However, it would seem reasonable to suggest that the local minimum on the body mode Q_2 will slow the decay of population to the 238 nm emission by at least an order of magnitude longer than that occurring on the waist mode. A quantitative comparison of the risetime on the calculated Q_2 mode with that observed on the 238 nm emission is difficult to make as the Franck–Condon spread in absorption will result in a distribution of rates. An experimental observation which should be mentioned in this regard, however, is that the intensity of the 238 nm emission was found[10] to be enhanced with 205.5 nm excitation while that of the 219 nm emission was greatest with 208.2 nm excitation. Conspicuously, the lower energy C emission is favored with high-energy excitation and the high-energy B emission is favored with low-energy excitation. From the overlay of the three potentials shown in the top panel of Fig. 3 for the breathing, body, and waist modes, it would appear, in line with observations, that the low-energy excitation at 208 nm accesses predominantly the waist mode, where the higher energy 219 nm emission is favored. 205.5 nm excitation predominately accesses the breathing mode which is entirely repulsive and will populate the lower energy body and waist modes equally.

B. High temperature

An experimental observation made[11] at high temperatures, $T>14$ K, was that the intensity of the 219 nm emission band could be put into the 238 nm band. The effect was completely reversible in that the original low-temperature spectrum was completely regained after a temperature cycle. A kinetics study[11] of this effect indicated that the process involved a barrier of $130.6\ \mathrm{cm}^{-1}$. In order to obtain theoretical predictions of the activation energy barriers for interconversion between the Jahn–Teller minima on the excited spin singlet state, potential-energy surfaces (PES) arising from the coupled $Q_2\times Q_3$ vibronic modes must be generated from the pair potentials calculations. For computational reasons this was achieved by repeating the Q_3 waist mode calculation for successive displacements along the Q_2 body mode.

A plot of the resulting surface is shown in Fig. 6. By obtaining the minimum energy of the waist mode for successive displacements along the body mode, the path of least energy on going from the minimum of the waist mode to the minimum of the body mode was identified. This path is shown in Fig. 6 by the location of the white arrows on the $Q_2\times Q_3$ potential-energy surface and the saddle point, the point of maximum energy on this path of least energy, is located at $Q_3=0.72$ and $Q_2=1.1$ Å. The former distance refers to the contraction of 4 Ar atoms from their original lattice positions towards the zinc atom, the latter to migration of the zinc atom from the substitutional site it originally occupies to a neighbouring octahedral interstitial site of the lattice.

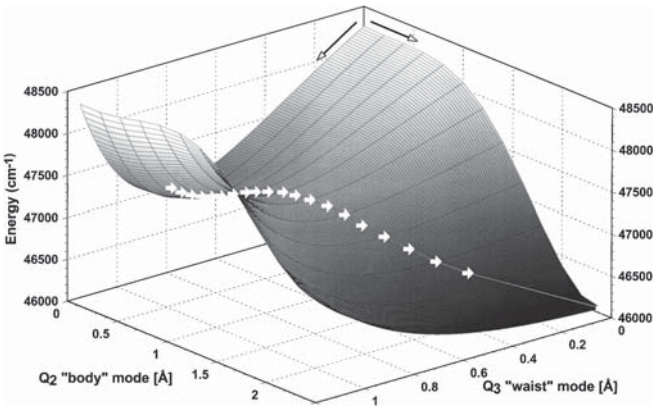

FIG. 6. Potential-energy surface (PES) calculated for the coupled body and waist modes (Q_2 and Q_3) in the Zn($^1P_1$)/Ar system. The region of the PES accessed in a Franck–Condon absorption from the ground state is located at $Q_2=0$ and $Q_3=0$ at the back of the diagram. At this position branching to the Q_2 and Q_3 modes, represented by the two black arrows, occurs leading to the C (238 nm) and B (219 nm) band emissions, respectively. A barrier of $396\ \mathrm{cm}^{-1}$ exists between the minimum of the waist mode and a saddle point located at $Q_2=1.1$ and $Q_3=0.72$ Å, on the surface shown. At high temperatures population which is initially routed along the steeper Q_3 mode can access the lower energy Q_2 mode by traversing this saddle point.

The saddle point is $396\ \mathrm{cm}^{-1}$ above the energy minimum of the waist mode. This energy is taken as the classical activation energy, E_C, for interconversion of population from the B (219 nm) to the C (238 nm) emitting level in the Zn–Ar system—a value which ignores zero-point energy (ZPE) in the waist mode and ZPE at the saddle point. To obtain a theoretical activation energy, E_0, for comparison with experimental observations, the vibrational frequencies of the waist mode, Q_3, at its energy minimum and at the saddle point are used to provide the zero-point energies. Taking the second derivatives of the Q_3 mode at the energy minimum and saddle point locations, $R=0.78$ and 0.72 Å, respectively, yields values of 97.12 and $70\ \mathrm{cm}^{-1}$ for their vibrational frequencies. Assuming that the zero-point energy is half the vibrational frequencies then the theoretical activation energy is $382\ \mathrm{cm}^{-1}$, $13.5\ \mathrm{cm}^{-1}$ less than the classical value. In spite of this correction the predicted barrier height is still about three times larger than the $130.6\ \mathrm{cm}^{-1}$ extracted from the Arrhenius plots.

C. Site occupancy in Zn–Ar

A possible reason for the poor agreement between the observed and predicted barrier heights in the Zn–Ar system is the placement of a zinc atom in a substitutional site of an

undisturbed substitutional site in solid Ar. The equilibrium internuclear separation of diatomic Zn·Ar in the ground electronic state is known to be 4.18 Å, considerably larger than that of Ar dimer which is only 3.76 Å. The long Zn·Ar bond length results in cramped occupancy of atomic zinc in a substitutional site of an undisturbed lattice.

To determine the geometry of isolation of Zn in Ar we have performed[14] a calculation which balances the maximum energy of interaction between the Zn atom in its electronic ground state and its 12 nearest Ar atoms while minimizing the resulting disruption arising from the displacement of the 12 Ar atoms. The $Zn \cdot Ar_{12}$ interaction is obtained from the symmetric breathing a_{1g} mode, which has an energy minimum at a cage size 0.43 Å larger than the substitutional site diameter of solid Ar. Radial expansion of the 12 Ar atoms in the $Zn \cdot Ar_{12}$ cubooctahedron induces two types of destabilization in the Ar lattice. One is the expansion of the 24 Ar–Ar nearest-neighbor bond lengths on the surface of the $Zn \cdot Ar_{12}$ cubo-octahedron, the other is the approach of each of these twelve Ar atoms to another nearest-neighbor Ar atom located on the radial axis containing the atomic Zn guest. For small displacements, the two terms contribute equally to the destabilization of the Ar lattice, while for displacements greater than 0.15 Å the latter repulsive term quickly dominates. By balancing the increased stabilization of the Zn·Ar interactions by expanding the $Zn \cdot Ar_{12}$ cubo-octahedron and the destabilisation thereby induced in the Ar lattice, it is found that the size of the site accommodating atomic zinc is 0.122 Å larger than an undistorted substitutional site of Ar. This expanded site results in a net destabilization of 144 cm^{-1} in the Ar lattice.

When the coupled $Q_2 \times Q_3$ $^1A_1$ potential-energy surface is re-generated with this 0.122 Å increase in the substitutional site size,[14] the barrier height was found to increase by 5 cm^{-1}. Thus we conclude that the size of the substitutional site accommodating the guest Zn atom in the Ar lattice has only a minor effect on the barrier height for Jahn–Teller interconversion on the excited singlet surface.

IV. CONCLUSIONS

The $Zn \cdot RG_{18}$ pair potential calculations of Ref. 8 have been extended from simulations of the energetics of the luminescence to include the dynamics observed on the excited singlet surface of the Zn–Ar system. In particular the existence of a risetime on the *C* (238 nm) emission band and its absence on the *B* (219 nm) band at low temperatures has been identified as arising from the a shallow gradient on the body modes potential and the steep gradient of the waist mode. Competitive decay rates of 2 and 1 ps calculated at the Franck–Condon accessible regions of the body Q_2 and waist Q_3 vibronic modes, respectively, leads to effective competition between these two vibronic modes, and thereby, to coexistence of the *C* band (238 nm) emission with the *B* band (219 nm). The presence of the quasi-bound region at 0.32 Å on the body mode introduces a bottleneck in the temporal evolution of the 238 nm emission, and hence, may be responsible for the risetime observed in this band.

The temperature dependence exhibited by the intensities of the *B* and *C* emission bands has been investigated by performing calculations of the coupled $Q_2 \times Q_3$ vibrational surfaces. Identification of a saddle point on the surface and calculation of the zero-point energies indicated qualitative agreement between the barrier height and the activation energy barrier extracted in the kinetic measurements. The reason for the discrepancy in the observed and calculated barrier heights is not immediately evident. It must however, be remembered that the theoretical value ignores any quantum mechanical tunneling which may become important for phonon levels near the top of the classical barrier.

[1] L. C. Balling, J. F. Dawson, M. D. Havey, and J. J. Wright, Phys. Rev. Lett. **43**, 435 (1979); J. F. Dawson and L. C. Balling, J. Chem. Phys. **71**, 836 (1979).
[2] C. Crepin and A. Tramer, J. Chem. Phys. **97**, 4772 (1992).
[3] S. Bililign, M. Gutowski, J. Simons, and W. H. Breckenridge, J. Chem. Phys. **99**, 3815 (1993).
[4] J. G. Kaup and W. H. Breckenridge, J. Phys. Chem. **99**, 13701 (1995).
[5] J. Zuniga, A. Bastida, A. Requena, N. Halberstadt, and J. Beswick, J. Chem. Phys. **98**, 1007 (1993).
[6] A. Bastida, J. Zuniga, A. Requena, B. Soep, N. Halberstadt, and J. Beswick, J. Chim. Phys. **92**, 384 (1995).
[7] S. Martrenchard-Barra, C. Jouvet, C. Lardeux-Dedonder, and D. Solgadi, J. Chem. Phys. **98**, 5281 (1993).
[8] J. G. McCaffrey and P. N. Kerins, J. Chem. Phys. **106**, 7885 (1997).
[9] The two modes were labeled ''body'' and ''waist'' because of their appearance in Fig. 1.
[10] V. A. Bracken, P. Gürtler, and J. G. McCaffrey, J. Chem. Phys. **107**, 5290 (1997).
[11] V. A. Bracken, P. N. Kerins, P. Gürtler, and J. G. McCaffrey, J. Chem. Phys. **107**, 5300 (1997).
[12] W. H. Breckenridge and J. G. McCaffrey, J. Chem. Phys. **109**, 3137 (1998), following paper.
[13] Similar to the a_{1g} vibrational mode of a square planar XY_4, D_{4h} polyatomic molecule, for which only the mass of one end *Y* atom is used to obtain the vibrational frequency, the effective reduced mass, μ', for the waist mode in the solid state Zn–Ar system is simply the atomic mass of Ar. See G. Herzberg, *Molecular Spectra and Molecular Structure, Vol. II, Infrared and Raman Spectra of Polyatomic Molecules* (Krieger, Florida, 1991), Chap. 4.
[14] P. N. Kerins, Masters Thesis, National Univ. of Ireland, Maynooth, 1997.